Published in final edited form as:
J Comp Neurol. 2009 September 1; 516(1): 1–19. doi:10.1002/cne.22058.

The morphology and spatial arrangement of astrocytes in the optic nerve head of the mouse

Daniel Sun, **Ming Lye-Barthel**, **Richard H. Masland**, and **Tatjana C. Jakobs**
Massachusetts General Hospital, Harvard Medical School, Boston, MA 02114

Abstract

We evaluated the shapes, numbers, and spatial distribution of astrocytes within the glial lamina, an astrocyte-rich region at the junction of the retina and optic nerve. A primary aim was to determine how the population of astrocytes, collectively, partitions the axonal space in this region. Astrocyte processes labeled with glial fibrillary acidic protein (GFAP) compartmentalize ganglion cell axons into bundles, forming “glial tubes”, and giving the glial architecture of the optic nerve head in transverse section a honeycomb appearance. The shapes of individual astrocytes were studied using transgenic mice that express enhanced green fluorescent protein in isolated astrocytes (hGFAPpr-EGFP). Within the glial lamina the astrocytes were transverse in orientation, with thick, smooth primary processes emanating from a cytoplasmic expansion of the soma. Spaces between the processes of neighboring astrocytes were spatially aligned, to form the apertures through which the bundles of optic axons pass. The processes of individual astrocytes were far-reaching – they could span most of the width of the nerve -and overlapped the anatomical domains of other near and distant astrocytes. Thus, astrocytes in the glial lamina do not tile: each astrocyte participates in ensheathing approximately one quarter of all of the axon bundles in the nerve, and each glial tube contains the processes of ~ 9 astrocytes. This raises the mechanistic question how, in glaucoma or other cases of nerve damage, the glial response can be confined to a circumscribed region where damage to axons has occurred.

Keywords

glial lamina; optic nerve; white matter astrocytes; GFP; glaucoma; ganglion cell axons

INTRODUCTION

The morphology of individual astrocytes and their diversity have long been known from work using the Golgi technique and electron microscopy (Ramon Y Cajal, 1909–1911; Klatzo, 1952). Immunocytochemical and single cell dye-injections have further characterized the three-dimensional appearance of these cells (Miller and Raff, 1984; Butt and Ransom, 1989; Butt and Ransom, 1993; Butt et al., 1994a; Butt et al., 1994b; Bushong et al., 2002). Astrocytes at different locations of the nervous system vary in the pattern of ramification of their processes and the contacts they make. The specialized endings of astrocyte processes form subpial and perivascular glia limitans (Landis and Reese, 1981; Landis and Reese, 1982; Gotow and Hashimoto, 1989), and they also have perinodal processes that contact axonal membranes at the Nodes of Ranvier (Raine, 1984; Waxman and Black, 1984; Suarez and Raff, 1989; Butt et al., 1994c). Their elaborate morphology

Correspondence: Tatjana Jakobs, Massachusets General Hospital, Thier 429, 50 Blossom Street, Boston, MA 02114, Tel: (+1) 617 724 7775, Jakobs@helix.mgh.harvard.edu.

allows them to be in close apposition to neuronal somas and dendrites, synapses, blood vessels and the margins of the nervous system.

Astrocytes have been assigned many functional roles. These include: providing structural rigidity, maintaining the extracellular environment, modulating synaptic function and plasticity, releasing neurotransmitters and energy substrates, regulating blood flow and assisting in the scarring and repair process (Haydon, 2001; Ullian et al., 2001; Nedergaard et al., 2003; Newman, 2003; Magistretti, 2006; Takano et al., 2006; Iadecola and Nedergaard, 2007; Rossi et al., 2007). However, the spatial relationship among astrocytes as populations have been little studied (Bushong et al., 2002; Halassa et al., 2007). How does the complex morphology of a single astrocyte contribute to the overall astrocyte array, and how does this array integrate into a fiber pathway?

Immunocytochemical detection of astrocyte markers does not reveal the extent of overlap between astrocyte territories. Glial fibrillary acidic protein (GFAP), the most commonly used immunocytochemical marker of astrocytes, is restricted to labeling the intermediate filaments, leaving much of the morphology unseen. In the brain, GFAP is reported to delineate only ~ 15% of the total volume of an astrocyte, grossly underestimating its full extent (Connor and Berkowitz, 1985; Bushong et al., 2002). Cytoplasmic markers such as S100 calcium binding protein β (S100β), glutamine synthetase (GS) or glutamate/aspartate transporter (GLAST) can reveal the fine processes, but produce a labeling pattern with little separation between neighboring astrocytes. Recent studies using single cell dye injections of neighboring astrocytes have revealed both the exquisite anatomical details of astrocytes and their spatial relationship. Use of this technique in the gray matter shows that protoplasmic astrocytes have minimal overlap between their processes, effectively tiling to form a patchwork of individual domains within the neuropil (Bushong et al., 2002; Ogata and Kosaka, 2002; Wilhelmsson et al., 2006; Halassa et al., 2007).

Here, we have studied the mosaic and tiling of astrocytes within the glial lamina, an astrocyte-rich region at the junction of the retina and optic nerve. We were particularly interested in this region because it appears to be the point of origin of axonal degeneration in glaucomatous neuropathy (Quigley, 1999; Jakobs et al., 2005; Howell et al., 2007; Buckingham et al., 2008; Soto et al., 2008). We used a transgenic mouse strain expressing enhanced green fluorescent protein in subsets of astrocytes (hGFAPpr-EGFP; (Nolte et al., 2001) to obtain a detailed three-dimensional visualization of the astrocytic organization within the glial lamina. In tissue from these animals the complete morphology of individual astrocytes can be imaged, along with the spatial relationship between neighboring astrocytes and other structural components (e.g., bundles of ganglion cell axon bundles, gap junctions, blood vessels, extracellular matrix components).

We report that the processes of astrocytes in the glial lamina surround and partition the axon bundles from one another, thus forming glial tubes through which run bundles of neighboring ganglion cell axons; they collectively form a honeycomb structure. Using the hGFAPpr-EGFP mice, we found that the processes of individual astrocytes can reach all the way across the nerve, overlapping substantially: every astrocyte potentially contacts nearly one quarter of all axon bundles within the nerve, and the wall of each glial tube is made up of the processes of several astrocytes. The projection of astrocytes to distant areas of the nerve raises questions about the mechanism of the astrocytic response to focal damage to axonal tracts, as occurs in glaucoma.

MATERIALS AND METHODS

Mouse strains

All animal procedures were approved by the Subcommittee on Research Animal Care of the Massachusetts General Hospital, Boston. Mice were housed on a 12 h light/dark cycle and received food and water ad libitum. Different lines of adult mice were used in this study: (1) wild type C57Bl/6, (2) transgenic mice in which astrocytes express enhanced green fluorescent protein (EGFP) under the control of the human glial fibrillary acidic protein (GFAP) promoter (hGFAPpr-EGFP). This transgenic strain has been established by injecting a 2.2 kb fragment of the human GFAP promoter fused to the EGFP gene into oocytes of FVB/N mice (Nolte et al., 2001). This promoter fragment has been shown to direct astrocyte-specific expression in transgenic mice (Brenner et al., 1994). The resulting strain displays bright labeling of individual astrocytes in the central and peripheral nervous system, the optic nerve and the retina. The green fluorescent cells in this mouse line are neither neurons nor oligodendrocytes (see Results and (Nolte et al., 2001; Emsley and Macklis, 2006). Heterozygous mice were used for all experiments involving transgenic animals; EGFP expression was confirmed by the illumination of the ears of young adult animals under a fluorescence dissecting microscope (peripheral glial cells are labeled brightly enough to be seen under these conditions). In addition, we used two more transgenic lines that express GFP retinal ganglion cells to trace axons in their course through the optic nerve (GFP-M and YFP-12). These lines are part of a series of strains generated by oocyte injections of genes coding for fluorescent proteins (GFP or YFP) under the control of a Thy1 promoter fragment (Feng et al., 2000). This promoter fragment has been shown to direct gene expression in neuronal cells (Vidal et al., 1990). In the case of GFP-M only ~30 ganglion cells per retina are labeled, whereas about 30% of all ganglion cells are labeled in YFP-12 (Feng et al., 2000; Kong et al., 2005; Jakobs et al., 2007).

Tissue preparation

Light-adapted mice were anesthetized with an intra-peritoneal injection of 100 mg/ml ketamine and 20 mg/ml xylazine and subsequently killed by an intra-cardiac injection of sodium pentobarbital. To obtain the optic nerve without causing structural damage, the animal's brain was exposed, and a razor blade was used to carefully cut away the brain immediately above the optic nerve and chiasm. The head was then immersed in fixative (4% paraformaldehyde) for 1 hour at room temperature and washed in 0.1 M phosphate buffered saline (PBS pH 7.4; 3 ×10 minutes). Following fixation, the remaining portion of the brain was gently detached from the optic nerve and chiasm. The orbital bones, retrobulbar tissue and ocular muscles were removed to isolate the globe and attached optic nerve.

The dura surrounding the optic nerve was delicately removed using fine dissection scissors. Using a razor blade, the globe was then dissected in two locations: (1) approximately 1–2 mm behind the limbus, and (2) approximately 1 mm anterior to the optic nerve head. Four small radial incisions were made in the remaining posterior retina, so that the retina could be flattened and the neural retina gently peeled away from the retinal pigment epithelium. The optic nerve was prepared in one of three ways: (1) the optic nerve was cut using a razor blade at the border of the unmyelinated and myelinated region, and then mounted in a slab of 4% agarose pointing upwards, or (2) the optic nerve was cut in half longitudinally using a razor blade and then mounted in a slab of 4% agarose with the cut surface facing up, or (3) the optic nerve was not sectioned at all and directly mounted in a slab of 4% agarose.

Immunohistochemistry

For immunohistochemistry, optic nerve sections were initially incubated in blocking solution (3% donkey serum, 0.5% Triton X-100, 0.01% NaN_3 in PBS) for 2 hours at room

temperature. The primary antibodies were diluted in 3% donkey serum, 0.5% Triton X-100, 0.01% NaN_3 in PBS. A list of the antibodies used is shown in Table 1. Optic nerves were incubated in the primary antibodies for at least seven days at 4°C, after which they were washed in PBS (pH 7.4, 3 × 10 minutes). Primary antibodies were visualized by the application of secondary antibodies conjugated with Alexa Fluor 350 (1:400, donkey anti-mouse, Molecular Probes, Eugene, OR), FITC (1:400, donkey anti-rabbit, Jackson ImmunoResearch, West Grove, PA) or rhodamine (1:400, donkey anti-rabbit and donkey anti-rat, Jackson ImmunoResearch). Secondary antibodies were applied for at least three days at 4°C and subsequently washed in PBS (pH 7.4, 3 × 10 minutes). The specificity of the secondary antibody was confirmed by leaving out the primary antibody or using a secondary antibody from a different species. These control experiments led to minimal background fluorescence. If counterstaining of cell nuclei was desired the retinas were incubated with 1 μm TO-PRO 3 iodide (T-3605, Invitrogen, Carlsbad, CA) for 20 min at room temperature.

Antibody characterization

The SMI32 antibody recognizes two bands of 200 and 180 kD in rodent brain extracts (Sternberger and Sternberger, 1983), and has been used to stain axons in normal and glaucomatous animals (Jakobs et al., 2005; Howell et al., 2007). The GFAP antibody recognized a single band of 46 kD m.w. on Western blots of rat brain (manufacturer's datasheet), and stained a pattern of cellular morphology and distribution in the mouse optic nerve that is identical with previous reports (Jakobs et al., 2005; Howell et al., 2007). The MBP antibody stained myelin sheaths consistent with that described in several studies (D'Urso et al., 1997; Pittier et al., 2005; Dugas et al., 2006). The NG2 antibody recognizes one band of 270–300 kD on Western blot and stained a population of cells with similar morphology to previous studies (Levine and Nishiyama, 1996) (Tekkok and Goldberg, 2001). The APC antibody recognizes one band at 312 kD on Western blot; in the optic nerve, this antibody stains oligodendrocytes (Bhat et al., 1996; Tekkok and Goldberg, 2001). The collagen type IV antibody produced a staining pattern consistent with that reported by (Johnson et al., 1996).

Anterograde dye-labeling of ganglion cell axons

The retina and optic nerve was fixed in 4% paraformaldehyde for 20 minutes. To label sectors of ganglion cells and trace their axons to bundles in the optic nerve, retinas with the optic nerve attached were flat mounted on 0.8 mm nitrocellulose filter paper (MF-Millipore membrane filter, #AABP04700, Millipore, Billerica, MA), with a hole for the optic nerve. Small crystals of 1,1'-dioctadecyl-3,3,3',3'-tetramethylindocarbocyanine perchlorate (DiI, #D282, Molecular Probes, Eugene, OR) were placed on the peripheral retina with a glass micropipette. The retina and optic nerve was kept suspended in a bath of PBS (pH 7.4) at 37°C in a humidified chamber for seven days, after which the optic nerve was isolated from the retina and embedded in 4% agarose for vibratome sectioning. The retina was mounted in Vectashield (Vector Laboratories, Burlingame, CA) on a slide and then cover-slipped for imaging on a confocal microscope.

Image acquisition and analysis

Images were acquired on a BioRad Radiance laser scanning confocal microscope equipped with Kr/Ar and CO_2 lasers mounted on a Zeiss Axioscope II. Water immersion lenses 25x/0.8 Plan Apochromat, 40x/1.2 C-Neofluar and 63x/1.4 C-Neofluar, (all from Carl Zeiss Microimaging, Inc.) were used. Emission filters were 522DF32 for EGFP/FITC, 680DF32 for TOPRO, and 605DF32 for rhodamine. Images were taken using the BioRad LaserSharp 2000 software (Version 5.0) and then exported into ImageJ (National Institute of Health, Bethesda, MD) or VolView (Kitware Inc., Clifton Park, NY) to produce either maximum

intensity projection images or volume reconstructions. Unless stated otherwise, all images are maximum intensity projections. The number of optical sections and step sizes used vary for each image. For the images in figure 1–figure 4, 20–70 optical sections were taken. For the images in figure 5– figure 9, 70–300 optical sections were taken. For all the figures, we used a step size of 0.3–0.5 μm. The highest number of optical sections taken was for figure 9D and F, where a reconstruction of the glial lamina was required. The brightness and contrast of the final images were adjusted using Adobe Photoshop CS2 (San Jose, CA), no other digital image processing was performed on the fluorescence micrographs.

Counts of the number of primary processes leaving the soma of an individual astrocyte were based on maximum intensity projection images. An estimation of the volume of the glial lamina was calculated by measuring the cross section of the optic nerve from microphotographs in SigmaScan (Jandel Scientific, San Rafael, CA) and multiplying by the length of the glial lamina. The pattern of GFAP labeling in longitudinal sections of the optic nerve head was used to determine the length of the glial lamina (~ 75 μm). We calculated the volume of the glial lamina to be ~ 0.004 mm^3. The number of astrocytes within this volume was determined by counting the number of TOPRO labeled nuclei excluding those that were recognized by their elongated shape to belong to endothelial cells. The volume of individual astrocytes was approximated by taking image stacks through single cells from hGFAPpr-EGFP mice, tracing the cells, and calculating the volume in MatLab (The Mathworks, Natick, MA) by a user-written routine. The dimensionless coverage factor is defined as (cells/mm^3) × (average volume of the cells in mm^3).

RESULTS

Expression profile of GFP in the optic nerve of hGFAPpr-EGFP mice

In agreement with earlier reports (Nolte et al., 2001), we found bright labeling of individual cells in the optic nerve and the retina. In the retina, these were exclusively Mueller cells, no neuronal cell type expressed GFP (data not shown, see also (Nolte et al., 2001). In the optic nerve, GFP-expressing cells were clearly of two kinds. One had the typical morphology of astrocytes. In immunostaining these cells were labeled by anti-GFAP antibodies, but not by antibodies against an oligodendrocyte marker (APC) or NG2. The other GFP-expressing cell type in the optic nerve was smaller and had multiple fine processes. These cells were immunoreactive for NG2, but not for markers of oligodendrocytes (APC; Figs. S1B–D), or astrocytes (GFAP; Figs. S1E–G). Within the myelinated region, NG2 immunoreactive cells were the most common cells expressing EGFP within the hGFAPpr-EGFP optic nerve (Fig. S1A). We shall not consider them further here. No other components of the optic nerve, axons, blood vessels and pia, showed any GFP expression.

Astrocytes of the optic nerve head form glial tubes

In mice, unmyelinated axons of retinal ganglion cells leave the globe through an opening in the sclera that lacks the collagenous meshwork that makes up the usual lamina cribrosa (Fujita et al., 2000; Morcos and Chan-Ling, 2000; May and Lutjen-Drecoll, 2002). Confirming earlier studies, we observed no staining for elastin or collagen in C57Bl/6 or in hGFAPpr-EGFP mice (data not shown). Myelination begins approximately 120–170 μm (n = 10) behind the sclera (Fig. 1).

Despite not having a classic lamina cribrosa, the unmyelinated region of the optic nerve is not unstructured. Instead it contains a characteristic meshwork of transversely oriented GFAP immunoreactive processes, forming a structure that has been named the “glial lamina” (Howell et al., 2007). Most nuclei within this region were transversely elongated and arranged in rows running perpendicular to the long axis of the nerve (Fig. 1B). Further

posteriorly, the cell nuclei were rounder in shape and aligned in longitudinal rows, parallel to the long axis of the nerve. The glial lamina begins at the level of the sclera and extends for 70–80 μm (n = 10) posteriorly, gradually ending before the axons become myelinated (Figs. 1C–E; an enlarged image of the glial lamina is shown in figure 3G). There were no oligodendrocytes or NG2 immunoreactive cells within the unmyelinated region of the optic nerve (Figs. 1F–H). These features are summarized in the schematic in the top right hand corner of figure 1.

The processes of astrocytes within the glial lamina partition neighboring ganglion cell axons into bundles, with multiple processes combining to form a short tube of astrocytic matter that ensheaths the bundle of axons as it runs longitudinally along the optic nerve head. The close-packing of the glial tubes gives the glial architecture within this region a honeycomb appearance (Figs. 2A–F; the dashed circle in panels D–F represents one such glial tube). The size of the glial tubes, and thus of the axon bundles that make up the honeycomb, decreases from anterior to posterior, concomitant with an increase in their number. They are largest in the region closest to the retina and gradually become smaller and more numerous towards the beginning of the myelinated region. This means that the axon bundles are progressively fractionated as they go from the large axon bundles anteriorly to the smaller more posterior ones.

The walls of the glial tubes are made up of multiple thick primary processes that lie alongside each other to ensheath the axon bundles (Figs. 2G–I; arrows). Additionally, numerous short fine processes arising from the primary process or cell body, traverse individual nerve bundles, forming second-order walls that subdivide the bundles into smaller units (Figs. 2G–I; arrowheads). These divisions become more frequent in the posterior part of the optic nerve. A single plane transverse section of the glial lamina shows that the walls of a glial tube may not necessarily contain cell nuclei on all its sides (Fig. 2J). Moreover, these nuclei are not arranged in any obvious pattern within the glial lamina and do not lie at the junctions of GFAP labeling (Fig. 2J; asterisks). The cell nuclei were large, elongated and irregular in shape.

Further posterior to the glial lamina, the organization of axons into bundles is lost. As in other mammals (Radius and Anderson, 1979), this transition is gradual, beginning soon after the glial lamina within the unmyelinated region of the nerve, and becoming complete at the level of the myelinated nerve. Here, astrocyte processes do not mix and lie beside each other; their processes are slender and appear straighter; there is less volume occupied by astrocytes; and there are no distinct glial tubes (Figs. 3A–F). Longitudinal sections of the optic nerve labeled for GFAP demonstrate the disorganization of the glial filaments further posteriorly along the optic nerve (Figs. 3G–I). On transverse section, the cell nuclei within this region are not arranged in any pattern and appear small and round, compared to those observed in the glial lamina (Fig. 3J).

The loss of organized axon bundles can be directly demonstrated by anterogradely labeling ganglion cell axons with the lipophilic carbocyanine dye DiI. When small crystals of DiI are placed onto the nerve fiber layer of the retina, the dye migrates in the axonal cell membrane into the optic nerve. Figure 4A–C shows transverse sections of the same optic nerve, either within the retina (panel A), directly behind the scleral opening (panel B), or ~ 100 μm behind the sclera (panel C). Figure 4D shows a second example in which transverse sections were made either behind the sclera (left image) or well within the myelinated region (right image). At the level of the glial lamina, discrete axon bundles are discernable (only a minor portion of all axon bundles are labeled because the DiI crystal was placed onto the peripheral retina, so only the axons from a sector comprising about a fourth of the retina came into contact with the dye). In the myelinated region, the axons have dispersed and

course towards the chiasm without an obvious topographic relationship (Horton et al., 1979; Radius and Anderson, 1979; Ogden et al., 1988). The bundled arrangement of axons within the optic nerve head region is also obvious in a longitudinal section (Fig. 4E; dashed square). Here, GFP labeled ganglion cell axon bundles are separated by astrocytes. Further posteriorly along the nerve, neighboring axon bundles are less separated and appear to coalesce together. Using a transgenic mouse that expresses GFP sparse populations of ganglion cell axons, we demonstrate that these axons can in fact disperse and deviate from their original location within the optic nerve (Fig. 4F; arrowheads). In this case, the axon began at a peripheral location within the optic nerve head, but shifted to a more central location as it traveled towards the chiasm.

Individual astrocytes of the optic nerve visualized in the hGAPpr-EGFP mice

Within the glial lamina, individual astrocytes had thick, elongated cell bodies and processes preferentially oriented transversely to the long axis of the optic nerve (Figs. 5A–C). This was consistent with the transverse arrangement of intermediate filaments demonstrated in the GFAP labeling pattern (Fig. 3G). In the 27 optic nerves examined, all of the astrocytes encountered in the glial lamina had this transverse orientation. The primary processes, of which there were typically 6–8 (n = 10), appeared to be mainly dense trunks emanating from a thick cytoplasmic extension of the soma. These processes were smooth and possessed very few higher order branches. They could span the entire width of the optic nerve, passing numerous near and distant axon bundles (Fig. 5D; arrowheads), to contact the pial wall or blood vessels via their bulbous endfeet (Figs. 5E, F and G). The same primary process could project processes to contact both the pial wall and blood vessels (Fig. 5G; arrows and arrowheads). Small, short longitudinal processes projected from the cell body and sometimes from the primary processes, passing for short distances before appearing to end freely in the nerve (Fig. 5C and E, arrowheads). Due to the overall curvature of these astrocytes (Figs. 5B and C), the profile of an individual transversely oriented astrocyte was roughly that of a baseball catcher’s mitt. A three-dimensional volume reconstruction of two astrocytes from within the glial lamina is shown in the supplementary material, including the single astrocyte in figure 5E (Movie S3 and Movie S4).

Astrocytes within the myelinated region of the optic nerve showed heterogeneous morphologies (Fig. 6– Fig 8), but had certain features in common. The processes of astrocytes extended in all directions. Thick primary branches typically ended at either the pial wall or on blood vessels via bulbous endfeet, whilst longitudinally oriented collateral branches emanated either from the primary processes, or from the cell body, and passed for a short distance before appearing to end freely in the nerve without any terminal specializations. No astrocyte extended processes exclusively to the pial wall or within the nerve. Processes bifurcated at intervals along their length and the caliber of individual processes of single astrocytes varied. Astrocytes exhibited processes that varied in their surface texture (e.g., smooth or undulating), and the degree of higher order branching, with some additionally showing many short fine offshoots. Smooth processes were typically long and straight whereas undulating processes had many small collaterals and offshoots.

Astrocytes in the optic nerve exhibit a wide spectrum of shapes and sizes (Butt et al., 1994b). We also observed clear examples of longitudinally and transversely oriented astrocytes, which have both their elongated cell bodies and processes projecting in the respective directions, but there were also astrocytes that showed characteristics of both forms, with processes projecting in both directions or in apparently random ones. There were many variations in the shapes of longitudinally oriented astrocytes. For example, some longitudinally oriented astrocytes possessed very few primary processes which were smooth, straight and had very few higher order branches (Figs. 6A and B), while others projected numerous primary processes exhibiting: (1) a dense network of short collaterals and fine

offshoots, giving the astrocytes a 'hairy' appearance (Figs. 6C–F), or (2) virtually no higher order branches (Figs. 6G and H). In all cases, these astrocytes had longitudinally elongated cell bodies. Transversely oriented astrocytes within the myelinated optic nerve were morphologically distinct from those found in the glial lamina. Some projected a thick extensive longitudinal process that ended with a specialized terminal (Figs. 7A and B; arrowheads). Others possessed a slender elongated cell body from which thick long primary processes projected directly to the pial wall. These astrocytes have very few higher order branches (Figs. 7C–E). There were many astrocytes that projected primary processes in: (1) both the longitudinal and transverse directions (Figs. 8A and B), and (2) in random directions (Figs. 8C and D). These astrocytes typically have round cell bodies. Some astrocytes lay directly along the pial wall. These astrocytes have elongated cell bodies in parallel with the long axis of the nerve (Figs. 8E and F). The collection of astrocytes we describe here is by no means complete and examination of different hGFAPpr-EGFP optic nerves revealed a large variety of morphologically different astrocytes. A gallery of additional examples is included in the supplementary material (Fig. S2).

The spatial network of astrocytes in the glial lamina

Each of the glial tubes (Figs. 9A and B; dashed circles) within the honeycomb arrangement is made up of the processes of numerous astrocytes (Figs. 9A and B; arrowheads). From the GFAP labeling pattern, it is unclear how the glial tubes are formed by the processes. How many astrocytes participate in forming the walls of a glial tube and how do these astrocytes arrange themselves? The requirement for more than one astrocyte to form a glial tube can be reasoned from the lack of glial tubes when single astrocytes are imaged (Fig. 5). The spatial relationship can be directly observed when fortuitously two or more neighboring astrocytes in the hGFAPpr-EGFP optic nerves express the EGFP label. We see that as the primary processes of each astrocyte project to contact the pial wall, they overlap with each other, forming holes through which it can be envisioned that the ganglion cell axons travel (Fig. 9C; dashed circles). Thick higher order branches also contribute in forming the walls of the glial tubes (Fig. 9C; arrow).

Because of the density of astrocytes (the glial lamina contains ~ 200 astrocytes in a volume of ~ 0.004 mm^3) and the fact that their processes usually span at least half the diameter of the nerve: (1) astrocytes within the glial lamina overlap in their spatial domains, (2) each astrocyte participates in forming the walls of numerous glial tubes, both near and distant, and (3) each glial tube in the honeycomb structure contains the processes of ~ 9 individual astrocytes, which originate from both near and distant locations (Table 1). Thus, each glial tube is not composed of a single astrocyte solely devoted to wrapping around a single bundle of axons. To determine the coverage factor of an individual astrocyte, we counted the number of axon bundles each of its processes passed through. We found that each astrocyte passes on average 24% of the total number of axons bundles within the nerve. In an example where there were many neighboring astrocytes expressing EGFP, in addition to processes, astrocyte cell bodies also contribute to making up the perimeter of the glial tubes (Figs. 9D and E). A three-dimensional volume reconstruction of figure 9E is included in the supplementary material (Movie. S5). Astrocytes within the glial lamina rarely project extensive longitudinal processes (Fig. 9F; right panel), so that they form sheets aligned transversely across the optic nerve (Figs. 9D and F, arrowheads).

Discussion

Confirming earlier studies, we found that the mouse optic nerve does not have a classic lamina cribrosa (Fujita et al., 2000; Morcos and Chan-Ling, 2000; May and Lutjen-Drecoll, 2002; Howell et al., 2007). The primary difference from primate optic nerves is the absence of the collagenous extracellular matrix that forms the "plates" of the lamina cribosa. Another

difference is that the transition zone between the unmyelinated and myelinated region of the nerve, which in primates is directly behind the lamina cribrosa (Oyama et al., 2006), is located further posteriorly in mice. Many other features are similar. Both primates and mice possess an unmyelinated region at the optic nerve head, in which the axons are surrounded by astrocytes. In both species, this unmyelinated region contains glial tubes that lie in an antero-posterior direction. These glial tubes are larger and less numerous at anterior locations of the nerve head (Ogden et al., 1988). Oligodendrocytes and NG2 expressing cells do not appear until the myelinated region of the nerve. Astrocytes in the optic nerve head can occupy as much as 50% of the tissue volume, whereas those in the optic nerve proper occupy 8–16% of tissue volume (Skoff et al., 1986). Both have various morphological types of astrocytes within the optic nerve head region. When transverse sections labeled with GFAP are observed, the glial lamina of the mouse optic nerve very much resembles the human lamina cribrosa, as both have an overall honeycomb appearance in which axon bundles travel through holes (Ogden et al., 1988). Most importantly, the optic axons in both cases are directly ensheathed by astrocytes. This is because the surface and sieve-like pores of the collagenous plates of the primate lamina cribosa are lined with astrocytes, separating the connective tissue septa from the axon bundles (Radius and Gonzales, 1981; Elkington et al., 1990; Ye and Hernandez, 1995; Trivino et al., 1996; Oyama et al., 2006).

Astrocyte heterogeneity

Astrocytes of the mouse optic nerve correspond to the white matter fibrous astrocytes of classical nomenclature. Fibrous astrocytes are less complex than protoplasmic astrocytes of the gray matter, and have fewer primary GFAP immunoreactive processes. Their processes are straighter and less branched than those of other glial types (Reichenbach and Wolburg, 2005). Based on the contacts these astrocytes make within the optic nerve, they appear to be capable of all the functions generally attributed to astrocytes, providing a communication pathway between the different elements within the region; the axons, blood vessels and the pial wall. All astrocytes have to some degree radial and longitudinal processes, numerous freely ending nerves that have been shown to contact axons at the Nodes of Ranvier (perinodal processes; (Raine, 1984; Waxman and Black, 1984; Butt et al., 1994c), and primary processes that contact the pia or blood vessels via their bulbous endfeet. For example, subpial astrocytes exhibited a morphology appropriate for a specialized role in the support and maintenance of the pia mater, but transverse, random and longitudinally oriented astrocytes also made contact with the pial wall. Similiarly, while longitudinally oriented astrocytes appear to be well suited for supporting the axons, as their processes run in parallel and project many finger-like processes, both random and transversely oriented astrocytes also contribute processes that end freely in the nerve.

In our study of astrocyte morphology we relied on a transgenic mouse model. The hGFAPpr-EGFP strain expresses GFP in many, but not all astrocytes (and NG2 cells), thus appearing as a “live Golgi stain”. This is an advantage because individual cells can be imaged clearly. However, it also is a limit to the interpretation of our results: there are many more cells stained in immunohistochemistry using anti-GFAP antibodies than there are cells expressing the fluorescent protein. This does not affect our conclusions. Our estimate of astrocyte coverage, for example, is based on nuclear staining, not on GFP expression. However, cells of a particular morphological type may be over- or underrepresented in our sample; and we cannot conclude that the frequency with which we encountered a particular morphological type reflects the frequency with which this cells occurs in vivo.

Astrocytes within the rodent optic nerve have been described to have three dominant forms based on the orientation of their primary processes with respect to the long axis of the nerve: transverse, random and longitudinal forms (Butt and Ransom, 1989; Butt et al., 1994a; Butt et al., 1994b). In agreement with these studies, we also observed many astrocytes that could

clearly be considered as being transversely or longitudinally oriented. However, we encountered much greater diversity in the shapes of the randomly oriented astrocytes. Qualitatively, there was no obvious strict morphological clustering of shapes. This variation confirms the notion that astrocytes within the rodent optic nerve form a single population in which the clearly transversely and longitudinally oriented astrocytes represent extreme morphological variants of the random form (Butt et al., 1994a; Butt et al., 1994b). Other studies of astrocytes, including those in the nerve fiber layer of the retina and rat fimbria have come to a similar conclusion, that astrocytes form a single morphological and multifunctional population (Ling et al., 1989; Chan-Ling and Stone, 1991; Suzuki and Raisman, 1992). Whether astrocytes of the optic nerve can be segregated based on their functional or molecular properties, as opposed to pure morphology, is unknown. Such heterogeneity has been reported for astrocytes of the hippocampus and for oligodendrocyte precursor glial cells (Steinhauser et al., 1992; Zhou and Kimelberg, 2001; Bachoo et al., 2004; Wallraff et al., 2004; Karadottir et al., 2008). The morphological diversity of astrocytes in the optic nerve has been suggested to result from the direct structural and functional interactions with its microenvironment, particularly during development, as the processes are induced to form specialized contacts with neighboring blood vessels, axons, the pia and/or other cell bodies (Foster et al., 1982; Blakemore and Smith, 1983; Sobue and Pleasure, 1984; Hatten, 1985; Sims et al., 1985; Butt and Ransom, 1993).

The organization of the glial lamina

The density and far reaching processes of glial lamina astrocytes mean that they cannot tile, but must overlap extensively into the spatial domains of neighboring astrocytes. This is in contrast to protoplasmic astrocytes of the gray matter (see below). Each astrocyte can influence approximately one quarter of all axon bundles in the nerve and each glial tube contains the processes of numerous astrocytes, from both near and distant locations. A single astrocyte is not confined to ensheathing a single bundle of axons. This overlap of processes also occurs between the astrocytes of the unmyelinated region. A functional consequence is that each astrocyte has the potential to communicate with and regulate the function of other distant astrocytes and axons, not just its neighbors. Along with the extensive gap junctional coupling between astrocytes (Nagy and Rash, 2000; Malone et al., 2007), one could imagine that the astrocyte meshwork forming the glial lamina acts as a single functional unit.

The purpose of having such a structure (whether it be the collagenous lamina cribrosa or the glial lamina) is unknown. It could be (1) to withstand the mechanical forces present at the junction of the retina and optic nerve (e.g., such as those imposed by the differences in intra-ocular and intra-cranial pressure). Astrocytes lining the human lamina cribrosa have been said to act as a ‘cushion’ between axons and the rigid collagenous structural material. (2) It could be a means to structurally support and segregate axon bundles. (The fasciculation of axon bundles may also function to disperse the compressive and stretching force to the optic nerve with eye movements.) It has been suggested that a dense collagenous network may simply be unnecessary in the smaller eye and nerve of the mouse. As the eye becomes larger and the optic nerve thicker, a collagenous lamina cribrosa may be needed to resist mechanical stress in response to pressure changes and eye movement (Fujita et al., 2000).

The response of astrocytes to injury

Astroglia are known to be a major player in the brain’s response to injury, both in grey and white matter (Pekny and Nilsson, 2005). In the gray matter of both the cortex and hippocampus, mature protoplasmic astrocytes form non-overlapping spatial domains that may also reflect independent functional domains. Three-dimensional volume reconstructions of adjacent astrocytes demonstrate that only the most peripheral processes of these astrocytes overlap with one another (Bushong et al., 2002; Ogata and Kosaka, 2002; Halassa

et al., 2007; Oberheim et al., 2008). This orderly pattern of organization – a phenomenon called 'tiling' - appears to occur throughout the gray matter of the brain and spinal cord. (Chan-Ling and Stone, 1991; Distler et al., 1991). Upon injury, astrocytes in the lesioned cortex and hippocampus remain within their domains, still showing minimal overlap (Wilhelmsson et al., 2006). Although the GFAP immunoreactive processes become thicker and longer (as GFAP immunoreactivity is seen in parts of the processes that were previously not immunoreactive), this hypertrophy does not affect the domain of tissue encompassed by processes of one astrocyte.

The optic nerve and its glial components, as a typical and accessible white matter tract, are well studied models of nerve injury and regeneration (Aguayo et al., 1991; Berry et al., 1996; Lorber et al., 2005; Benowitz and Yin, 2008; Berry et al., 2008). It well known that the glial scar that forms at the site of injury actively prevents axons from growing back and reinnervating their targets and therefore presents a major roadblock to regenerative therapy (Silver and Miller, 2004; Tan et al., 2005; Fitch and Silver, 2008). Glaucoma can also be considered a disease of a white matter tract, albeit one containing a unique, specialized structure - the lamina cribrosa in primates and the glial lamina in rodents - that may play a special role (Quigley et al., 1981; Howell et al., 2007; Nickells, 2007).

Glial reactivity in glaucoma first occurs in discrete focal regions (Danias et al., 2003; Jakobs et al., 2005; Schlamp et al., 2006). This focal region of loss is filled in by intense GFAP labeling, indicating classic glial reactivity (Howell et al., 2007). Our findings on the morphology of individual astrocytes and their spatial distribution raise the question: How can the glial response be confined to circumscribed regions of the optic nerve? (Figure 10). Damage that affects an individual bundle of nerve fibers would be expected to trigger a response in all of the astrocytes that ensheath that particular axon bundle. And yet, although process of those astrocytes reach distant locations across the optic nerve, the glial response to injury appears to remain local. This seems to imply a great specificity of reaction within an individual astrocyte, such that the reactive changes by an astrocyte are restricted to a limited region of that cell. Alternatively, the cells could remodel in a more extensive way, perhaps in combination with cell migration and/or cell division. These possibilities are shown schematically in figure 10.

Supplementary Material

Refer to Web version on PubMed Central for supplementary material.

Acknowledgments

We thank Prof. Helmut Kettenmann, Max-Delbrück-Centrum, Berlin, Germany for kindly providing the hGFAPpr-GFP mouse line. Supported by NIH grant R01-EY017169. RHM is a Senior Investigator of Research to Prevent Blindness.

References

Aguayo AJ, Rasminsky M, Bray GM, Carbonetto S, McKerracher L, Villegas-Perez MP, Vidal-Sanz M, Carter DA. Degenerative and regenerative responses of injured neurons in the central nervous system of adult mammals. Philos Trans R Soc Lond B Biol Sci. 1991; 331(1261):337–343. [PubMed: 1677478]

Bachoo RM, Kim RS, Ligon KL, Maher EA, Brennan C, Billings N, Chan S, Li C, Rowitch DH, Wong WH, DePinho RA. Molecular diversity of astrocytes with implications for neurological disorders. Proc Natl Acad Sci U S A. 2004; 101(22):8384–8389. [PubMed: 15155908]

Benowitz L, Yin Y. Rewiring the injured CNS: lessons from the optic nerve. Exp Neurol. 2008; 209(2):389–398. [PubMed: 17610877]

Berry M, Ahmed Z, Lorber B, Douglas M, Logan A. Regeneration of axons in the visual system. Restor Neurol Neurosci. 2008; 26(2–3):147–174. [PubMed: 18820408]

Berry M, Carlile J, Hunter A. Peripheral nerve explants grafted into the vitreous body of the eye promote the regeneration of retinal ganglion cell axons severed in the optic nerve. J Neurocytol. 1996; 25(2):147–170. [PubMed: 8699196]

Bhat RV, Axt KJ, Fosnaugh JS, Smith KJ, Johnson KA, Hill DE, Kinzler KW, Baraban JM. Expression of the APC tumor suppressor protein in oligodendroglia. Glia. 1996; 17(2):169–174. [PubMed: 8776583]

Blakemore WF, Smith KJ. Node-like axonal specializations along demyelinated central nerve fibres: ultrastructural observations. Acta Neuropathol. 1983; 60(3–4):291–296. [PubMed: 6613537]

Brenner M, Kisseberth WC, Su Y, Besnard F, Messing A. GFAP promoter directs astrocyte-specific expression in transgenic mice. J Neurosci. 1994; 14(3 Pt 1):1030–1037. [PubMed: 8120611]

Buckingham BP, Inman DM, Lambert W, Oglesby E, Calkins DJ, Steele MR, Vetter ML, Marsh-Armstrong N, Horner PJ. Progressive ganglion cell degeneration precedes neuronal loss in a mouse model of glaucoma. J Neurosci. 2008; 28(11):2735–2744. [PubMed: 18337403]

Bushong EA, Martone ME, Jones YZ, Ellisman MH. Protoplasmic astrocytes in CA1 stratum radiatum occupy separate anatomical domains. J Neurosci. 2002; 22(1):183–192. [PubMed: 11756501]

Butt AM, Colquhoun K, Berry M. Confocal imaging of glial cells in the intact rat optic nerve. Glia. 1994a; 10(4):315–322. [PubMed: 7520025]

Butt AM, Colquhoun K, Tutton M, Berry M. Three-dimensional morphology of astrocytes and oligodendrocytes in the intact mouse optic nerve. J Neurocytol. 1994b; 23(8):469–485. [PubMed: 7527074]

Butt AM, Duncan A, Berry M. Astrocyte associations with nodes of Ranvier: ultrastructural analysis of HRP-filled astrocytes in the mouse optic nerve. J Neurocytol. 1994c; 23(8):486–499. [PubMed: 7983475]

Butt AM, Ransom BR. Visualization of oligodendrocytes and astrocytes in the intact rat optic nerve by intracellular injection of lucifer yellow and horseradish peroxidase. Glia. 1989; 2(6):470–475. [PubMed: 2531727]

Butt AM, Ransom BR. Morphology of astrocytes and oligodendrocytes during development in the intact rat optic nerve. J Comp Neurol. 1993; 338(1):141–158. [PubMed: 8300897]

Chan-Ling T, Stone J. Factors determining the migration of astrocytes into the developing retina: migration does not depend on intact axons or patent vessels. J Comp Neurol. 1991; 303(3):375–386. [PubMed: 2007655]

Connor JR, Berkowitz EM. A demonstration of glial filament distribution in astrocytes isolated from rat cerebral cortex. Neuroscience. 1985; 16(1):33–44. [PubMed: 2423916]

D'Urso D, Schmalenbach C, Zoidl G, Prior R, Muller HW. Studies on the effects of altered PMP22 expression during myelination in vitro. J Neurosci Res. 1997; 48(1):31–42. [PubMed: 9086179]

Danias J, Lee KC, Zamora MF, Chen B, Shen F, Filippopoulos T, Su Y, Goldblum D, Podos SM, Mittag T. Quantitative analysis of retinal ganglion cell (RGC)loss in aging DBA/2NNia glaucomatous mice: comparison with RGC loss in aging C57/BL6 mice. Invest Ophthalmol Vis Sci. 2003; 44(12):5151–5162. [PubMed: 14638711]

Distler C, Dreher Z, Stone J. Contact spacing among astrocytes in the central nervous system: an hypothesis of their structural role. Glia. 1991; 4(5):484–494. [PubMed: 1834565]

Dugas JC, Tai YC, Speed TP, Ngai J, Barres BA. Functional genomic analysis of oligodendrocyte differentiation. J Neurosci. 2006; 26(43):10967–10983. [PubMed: 17065439]

Elkington AR, Inman CB, Steart PV, Weller RO. The structure of the lamina cribrosa of the human eye: an immunocytochemical and electron microscopical study. Eye. 1990; 4(Pt 1):42–57. [PubMed: 2182351]

Emsley JG, Macklis JD. Astroglial heterogeneity closely reflects the neuronal-defined anatomy of the adult murine CNS. Neuron Glia Biol. 2006; 2(3):175–186. [PubMed: 17356684]

Feng G, Mellor RH, Bernstein M, Keller-Peck C, Nguyen QT, Wallace M, Nerbonne JM, Lichtman JW, Sanes JR. Imaging neuronal subsets in transgenic mice expressing multiple spectral variants of GFP. Neuron. 2000; 28(1):41–51. [PubMed: 11086982]

Fitch MT, Silver J. CNS injury, glial scars, and inflammation: Inhibitory extracellular matrices and regeneration failure. Exp Neurol. 2008; 209(2):294–301. [PubMed: 17617407]

Foster RE, Connors BW, Waxman SG. Rat optic nerve: electrophysiological, pharmacological and anatomical studies during development. Brain Res. 1982; 255(3):371–386. [PubMed: 7066695]

Fujita Y, Imagawa T, Uehara M. Comparative study of the lamina cribrosa and the pial septa in the vertebrate optic nerve and their relationship to the myelinated axons. Tissue Cell. 2000; 32(4): 293–301. [PubMed: 11145012]

Gotow T, Hashimoto PH. Developmental alterations in membrane organization of rat subpial astrocytes. J Neurocytol. 1989; 18(6):731–747. [PubMed: 2621474]

Halassa MM, Fellin T, Takano H, Dong JH, Haydon PG. Synaptic islands defined by the territory of a single astrocyte. J Neurosci. 2007; 27(24):6473–6477. [PubMed: 17567808]

Hatten ME. Neuronal regulation of astroglial morphology and proliferation in vitro. J Cell Biol. 1985; 100(2):384–396. [PubMed: 3881455]

Haydon PG. GLIA: listening and talking to the synapse. Nat Rev Neurosci. 2001; 2(3):185–193. [PubMed: 11256079]

Horton JC, Greenwood MM, Hubel DH. Non-retinotopic arrangement of fibres in cat optic nerve. Nature. 1979; 282(5740):720–722. [PubMed: 514350]

Howell GR, Libby RT, Jakobs TC, Smith RS, Phalan FC, Barter JW, Barbay JM, Marchant JK, Mahesh N, Porciatti V, Whitmore AV, Masland RH, John SW. Axons of retinal ganglion cells are insulted in the optic nerve early in DBA/2J glaucoma. J Cell Biol. 2007; 179(7):1523–1537. [PubMed: 18158332]

Iadecola C, Nedergaard M. Glial regulation of the cerebral microvasculature. Nat Neurosci. 2007; 10(11):1369–1376. [PubMed: 17965657]

Jakobs TC, Ben Y, Masland RH. Expression of mRNA for glutamate receptor subunits distinguishes the major classes of retinal neurons, but is less specific for individual cell types. Mol Vis. 2007; 13:933–948. [PubMed: 17653033]

Jakobs TC, Libby RT, Ben Y, John SW, Masland RH. Retinal ganglion cell degeneration is topological but not cell type specific in DBA/2J mice. J Cell Biol. 2005; 171(2):313–325. [PubMed: 16247030]

Johnson EC, Morrison JC, Farrell S, Deppmeier L, Moore CG, McGinty MR. The effect of chronically elevated intraocular pressure on the rat optic nerve head extracellular matrix. Exp Eye Res. 1996; 62(6):663–674. [PubMed: 8983948]

Karadottir R, Hamilton NB, Bakiri Y, Attwell D. Spiking and nonspiking classes of oligodendrocyte precursor glia in CNS white matter. Nat Neurosci. 2008; 11(4):450–456. [PubMed: 18311136]

Klatzo I. A study of glia by the Golgi method. Lab Invest. 1952; 1(3):345–350. [PubMed: 14955970]

Kong JH, Fish DR, Rockhill RL, Masland RH. Diversity of ganglion cells in the mouse retina: Unsupervised morphological classification and its limits. J Comp Neurol. 2005; 489(3):293–310. [PubMed: 16025455]

Landis DM, Reese TS. Membrane structure in mammalian astrocytes: a review of freeze-fracture studies on adult, developing, reactive and cultured astrocytes. J Exp Biol. 1981; 95:35–48. [PubMed: 7038024]

Landis DM, Reese TS. Regional organization of astrocytic membranes in cerebellar cortex. Neuroscience. 1982; 7(4):937–950. [PubMed: 7099425]

Levine JM, Nishiyama A. The NG2 chondroitin sulfate proteoglycan: a multifunctional proteoglycan associated with immature cells. Perspect Dev Neurobiol. 1996; 3(4):245–259. [PubMed: 9117258]

Ling TL, Mitrofanis J, Stone J. Origin of retinal astrocytes in the rat: evidence of migration from the optic nerve. J Comp Neurol. 1989; 286(3):345–352. [PubMed: 2768562]

Lorber B, Berry M, Logan A. Lens injury stimulates adult mouse retinal ganglion cell axon regeneration via both macrophage- and lens-derived factors. Eur J Neurosci. 2005; 21(7):2029–2034. [PubMed: 15869497]

Magistretti PJ. Neuron-glia metabolic coupling and plasticity. J Exp Biol. 2006; 209(Pt 12):2304–2311. [PubMed: 16731806]

Malone P, Miao H, Parker A, Juarez S, Hernandez MR. Pressure induces loss of gap junction communication and redistribution of connexin 43 in astrocytes. Glia. 2007; 55(10):1085–1098. [PubMed: 17551925]

May CA, Lutjen-Drecoll E. Morphology of the murine optic nerve. Invest Ophthalmol Vis Sci. 2002; 43(7):2206–2212. [PubMed: 12091418]

Miller RH, Raff MC. Fibrous and protoplasmic astrocytes are biochemically and developmentally distinct. J Neurosci. 1984; 4(2):585–592. [PubMed: 6366155]

Morcos Y, Chan-Ling T. Concentration of astrocytic filaments at the retinal optic nerve junction is coincident with the absence of intra-retinal myelination: comparative and developmental evidence. J Neurocytol. 2000; 29(9):665–678. [PubMed: 11353290]

Nagy JI, Rash JE. Connexins and gap junctions of astrocytes and oligodendrocytes in the CNS. Brain Res Brain Res Rev. 2000; 32(1):29–44. [PubMed: 10751655]

Nedergaard M, Ransom B, Goldman SA. New roles for astrocytes: redefining the functional architecture of the brain. Trends Neurosci. 2003; 26(10):523–530. [PubMed: 14522144]

Newman EA. New roles for astrocytes: regulation of synaptic transmission. Trends Neurosci. 2003; 26(10):536–542. [PubMed: 14522146]

Nickells RW. From ocular hypertension to ganglion cell death: a theoretical sequence of events leading to glaucomac. Can J Ophthalmol. 2007; 42(2):278–287. [PubMed: 17392853]

Nolte C, Matyash M, Pivneva T, Schipke CG, Ohlemeyer C, Hanisch UK, Kirchhoff F, Kettenmann H. GFAP promoter-controlled EGFP-expressing transgenic mice: a tool to visualize astrocytes and astrogliosis in living brain tissue. Glia. 2001; 33(1):72–86. [PubMed: 11169793]

Oberheim NA, Tian GF, Han X, Peng W, Takano T, Ransom B, Nedergaard M. Loss of astrocytic domain organization in the epileptic brain. J Neurosci. 2008; 28(13):3264–3276. [PubMed: 18367594]

Ogata K, Kosaka T. Structural and quantitative analysis of astrocytes in the mouse hippocampus. Neuroscience. 2002; 113(1):221–233. [PubMed: 12123700]

Ogden TE, Duggan J, Danley K, Wilcox M, Minckler DS. Morphometry of nerve fiber bundle pores in the optic nerve head of the human. Exp Eye Res. 1988; 46(4):559–568. [PubMed: 3384014]

Oyama T, Abe H, Ushiki T. The connective tissue and glial framework in the optic nerve head of the normal human eye: light and scanning electron microscopic studies. Arch Histol Cytol. 2006; 69(5):341–356. [PubMed: 17372390]

Pekny M, Nilsson M. Astrocyte activation and reactive gliosis. Glia. 2005; 50(4):427–434. [PubMed: 15846805]

Pittier R, Sauthier F, Hubbell JA, Hall H. Neurite extension and in vitro myelination within three-dimensional modified fibrin matrices. J Neurobiol. 2005; 63(1):1–14. [PubMed: 15616962]

Quigley HA. Neuronal death in glaucoma. Prog Retin Eye Res. 1999; 18(1):39–57. [PubMed: 9920498]

Quigley HA, Addicks EM, Green WR, Maumenee AE. Optic nerve damage in uman glaucoma. II. The site of injury and susceptibility to damage. Arch phthalmol. 1981; 99(4):635–649.

Radius RL, Anderson DR. The course of axons through the retina and optic nerve ead. Arch Ophthalmol. 1979; 97(6):1154–1158. [PubMed: 109071]

Radius RL, Gonzales M. Anatomy of the lamina cribrosa in human eyes. Arch phthalmol. 1981; 99(12):2159–2162.

Raine CS. On the association between perinodal astrocytic processes and the ode of Ranvier in the C.N.S. J Neurocytol. 1984; 13(1):21–27. [PubMed: 6707711]

Ramon Y, Cajal S. Histologie du Systeméme Nerveux Del'homme et des ertébrés. Madrid. Consejo Superior de Investigaciones Cientificas. 1909–1911

Reichenbach, A.; Wolburg, H. Astrocytes and ependymal glia. In: Kettenman, H.; Ransom, BR., editors. Neuroglia. 2 ed. New York: Oxford University Press; 2005. p. 19-35.

Rossi DJ, Brady JD, Mohr C. Astrocyte metabolism and signaling during brain schemia. Nat Neurosci. 2007; 10(11):1377–1386. [PubMed: 17965658]

Schlamp CL, Li Y, Dietz JA, Janssen KT, Nickells RW. Progressive ganglon cell loss and optic nerve degeneration in DBA/2J mice is variable and asymmetric. BMC Neurosci. 2006; 7(1):66. [PubMed: 17018142]

Silver J, Miller JH. Regeneration beyond the glial scar. Nat Rev Neurosci. 2004; 5(2):146–156. [PubMed: 14735117]

Sims TJ, Waxman SG, Black JA, Gilmore SA. Perinodal astrocytic processes at odes of Ranvier in developing normal and glial cell deficient rat spinal cord. Brain Res. 1985; 337(2):321–331. [PubMed: 4027576]

Skoff, R.; Knapp, PE.; Bartlett, WP. Astrocyte diversity in the optic nerve: a cytoarchitectural study. In: Fedoroff, S.; Vernadakis, A., editors. Astrocytes. New York: Academic Press; 1986. p. 269-291.

Sobue G, Pleasure D. Astroglial proliferation and phenotype are modulated by neuronal plasma membrane. Brain Res. 1984; 324(1):175–179. [PubMed: 6518388]

Soto I, Oglesby E, Buckingham BP, Son JL, Roberson ED, Steele MR, Inman DM, Vetter ML, Horner PJ, Marsh-Armstrong N. Retinal Ganglion Cells Downregulate Gene Expression and Lose Their Axons within the Optic Nerve Head in a Mouse Glaucoma Model. J Neurosci. 2008; 28(2):548–561. [PubMed: 18184797]

Steinhauser C, Berger T, Frotscher M, Kettenmann H. Heterogeneity in the Membrane Current Pattern of Identified Glial Cells in the Hippocampal Slice. Eur J Neurosci. 1992; 4(6):472–484. [PubMed: 12106333]

Sternberger LA, Sternberger NH. Monoclonal antibodies distinguish phosphorylated and nonphosphorylated forms of neurofilaments in situ. Proc Natl Acad Sci U S A. 1983; 80(19): 6126–6130. [PubMed: 6577472]

Suarez I, Raff MC. Subpial and perivascular astrocytes associated with nodes of Ranvier in the rat optic nerve. J Neurocytol. 1989; 18(5):577–582. [PubMed: 2614479]

Suzuki M, Raisman G. The glial framework of central white matter tracts: segmented rows of contiguous interfascicular oligodendrocytes and solitary astrocytes give rise to a continuous meshwork of transverse and longitudinal processes in the adult rat fimbria. Glia. 1992; 6(3):222–235. [PubMed: 1478731]

Takano T, Tian GF, Peng W, Lou N, Libionka W, Han X, Nedergaard M. Astrocyte-mediated control of cerebral blood flow. Nat Neurosci. 2006; 9(2):260–267. [PubMed: 16388306]

Tan AM, Zhang W, Levine JM. NG2: a component of the glial scar that inhibits axon growth. J Anat. 2005; 207(6):717–725. [PubMed: 16367799]

Tekkok SB, Goldberg MP. Ampa/kainate receptor activation mediates hypoxic oligodendrocyte death and axonal injury in cerebral white matter. J Neurosci. 2001; 21(12):4237–4248. [PubMed: 11404409]

Trivino A, Ramirez JM, Salazar JJ, Ramirez AI, Garcia-Sanchez J. Immunohistochemical study of human optic nerve head astroglia. Vision Res. 1996; 36(14):2015–2028. [PubMed: 8776468]

Ullian EM, Sapperstein SK, Christopherson KS, Barres BA. Control of synapse number by glia. Science. 2001; 291(5504):657–661. [PubMed: 11158678]

Vidal M, Morris R, Grosveld F, Spanopoulou E. Tissue-specific control elements of the Thy-1 gene. Embo J. 1990; 9(3):833–840. [PubMed: 1968831]

Wallraff A, Odermatt B, Willecke K, Steinhauser C. Distinct types of astroglial cells in the hippocampus differ in gap junction coupling. Glia. 2004; 48(1):36–43. [PubMed: 15326613]

Waxman SG, Black JA. Freeze-fracture ultrastructure of the perinodal astrocyte and associated glial junctions. Brain Res. 1984; 308(1):77–87. [PubMed: 6434150]

Wilhelmsson U, Bushong EA, Price DL, Smarr BL, Phung V, Terada M, Ellisman MH, Pekny M. Redefining the concept of reactive astrocytes as cells that remain within their unique domains upon reaction to injury. Proc Natl Acad Sci U S A. 2006; 103(46):17513–17518. [PubMed: 17090684]

Ye H, Hernandez MR. Heterogeneity of astrocytes in human optic nerve head. J Comp Neurol. 1995; 362(4):441–452. [PubMed: 8636460]

Zhou M, Kimelberg HK. Freshly isolated hippocampal CA1 astrocytes comprise two populations differing in glutamate transporter and AMPA receptor expression. J Neurosci. 2001; 21(20):7901–7908. [PubMed: 11588163]

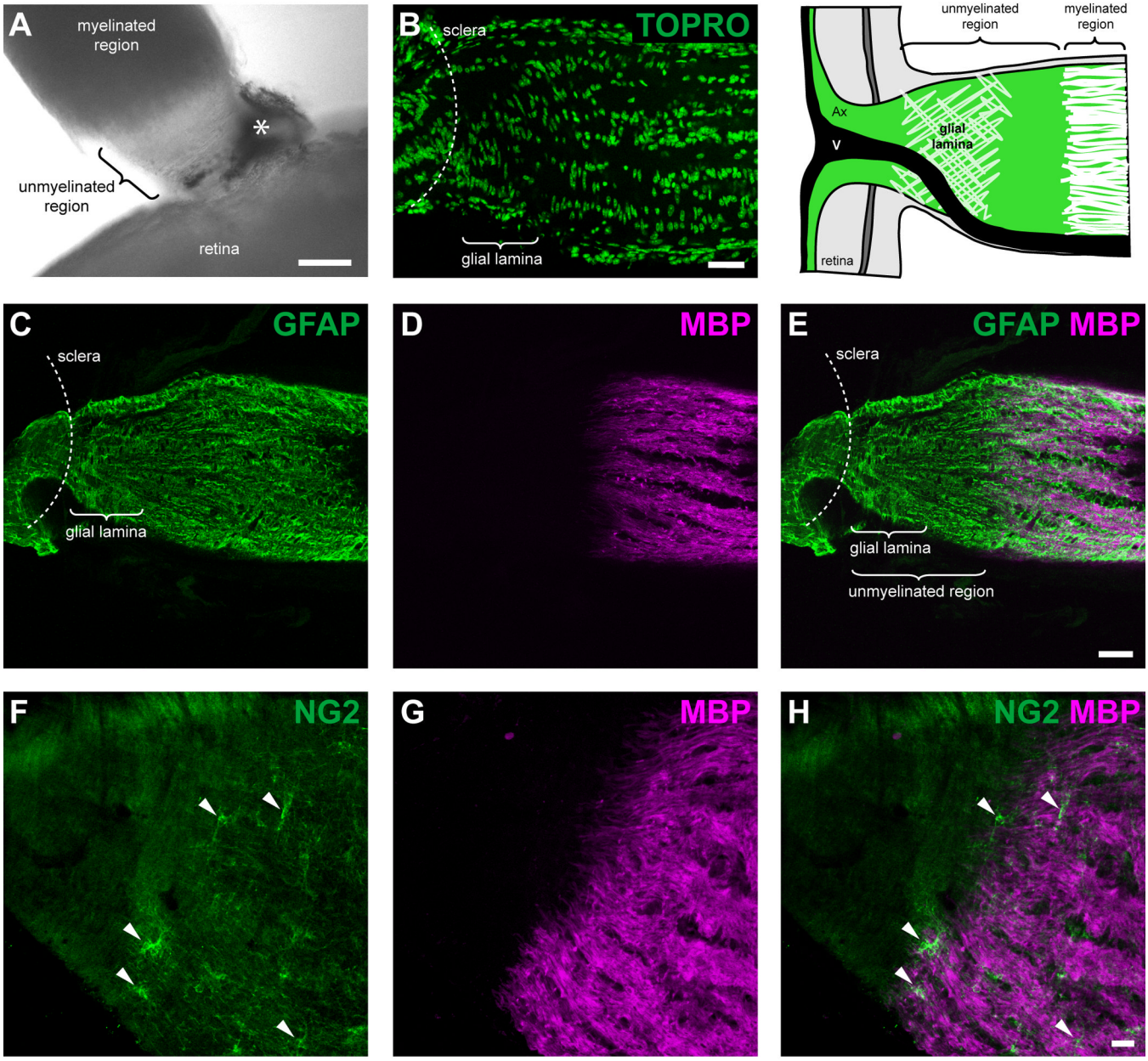

Fig. 1.

The unmyelinated region of the mouse optic nerve contains the glial lamina. (A) An image taken with an inverted light microscope demonstrates that myelination of the axons begins approximately 120–170 μm behind the sclera. Note the transparency of the unmyelinated region. The asterisk depicts a remnant of the sclera/retinal pigment epithelium. (B) TOPRO staining shows that most of the cell nuclei within the glial lamina were transversely elongated, whilst further posteriorly, the nuclei were rounder in shape and aligned in longitudinal rows parallel to the long axis of the nerve. Colocalization of the GFAP (C) and MBP (D) labeling pattern shows the transition between the unmyelinated and myelinated region of the optic nerve (E). The glial lamina was defined as the region showing dense transversely oriented intermediate filaments that were labeled with GFAP (an enlarged image of the glial lamina is shown in figure 3G). The glial lamina begins at the level of the sclera and extends for 70–80 μm, gradually ending before the axons become myelinated.

The schematic at the top right hand corner of the figure demonstrates the position of the major elements within the optic nerve head (adapted from Howell et al., 2007). Colocalization of the NG2 (F) and MBP (G) labeling pattern shows that the unmyelinated region is devoid of NG2 immunoreactive cells (F and H, arrowheads) and oligodendrocytes. Ax, axons; V, blood vessel. Scale bar = 100 μm in panel A; 40 μm in panel B; 40 μm in panel E (applies to panels C–E); 20 μm in panel H (applies to panels F–H).

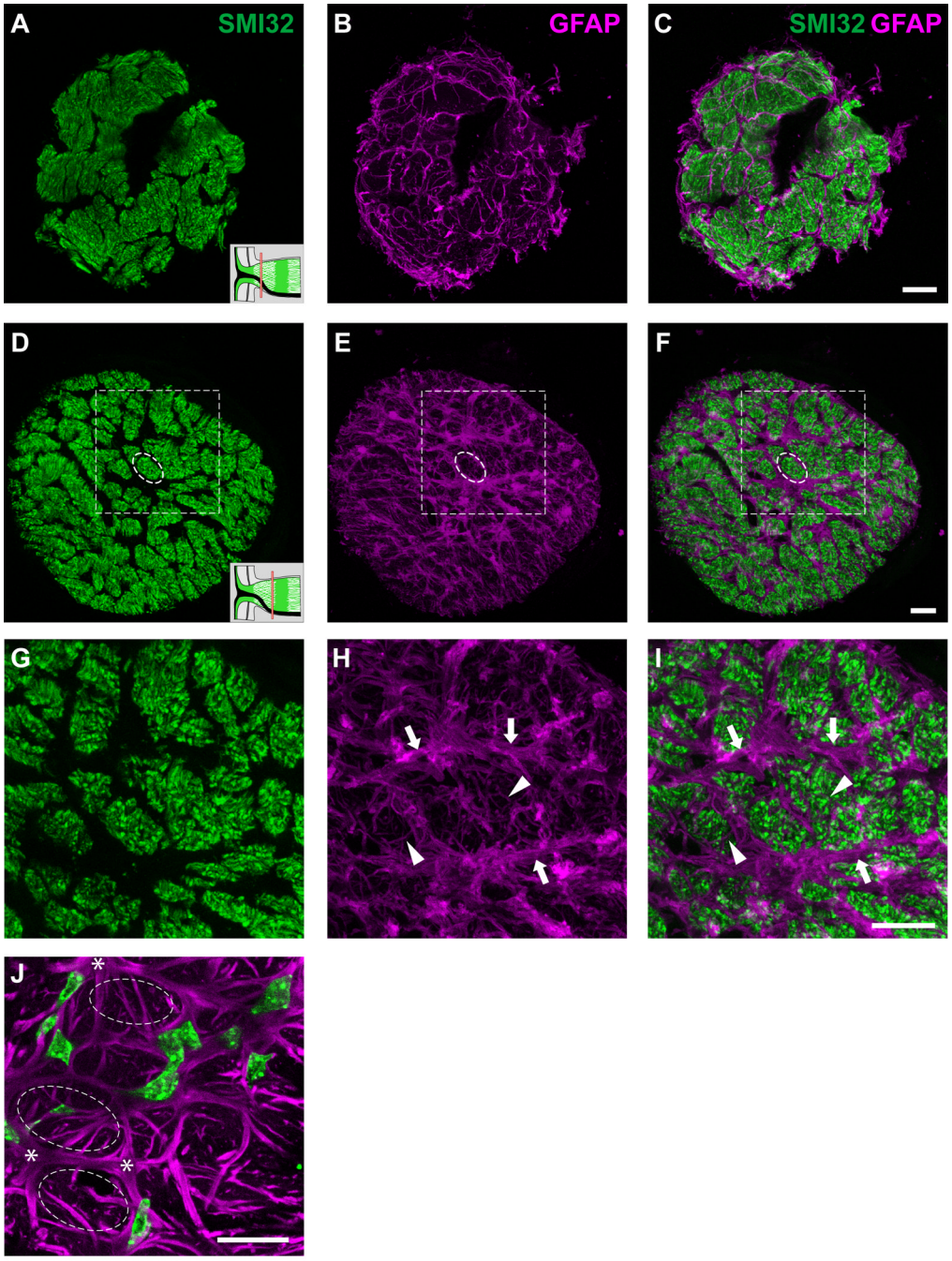

Fig. 2.

Transverse sections of the optic nerve labeled for SMI32 (A, D, G) and GFAP (B, E, H). Panels C, F and I show the colocalization pattern. The schematic of the optic nerve head in the lower right-hand corner of panels A and D indicate where along the optic nerve the transverse sections have been made (red bars). Within the glial lamina, GFAP labeled processes segregate axons into distinct bundles of various shapes and sizes (larger bundles are seen in sections close to the sclera, smaller and more numerous bundles further away), forming glial tubes (D–F; dashed circle). Panels G–I show an enlargement of the area within the dashed square in panels D–F. The walls of the glial tubes are made up of thick processes from many astrocytes (G–I; arrows). Additionally, small fine processes traverse into

individual nerve bundles (G–I, arrowheads). (J) Single confocal transverse section of the glial lamina labeled for GFAP and TOPRO. Within a single focal plane, the wall of a glial tube (dashed circles) is not necessarily surrounded by cell nuclei. The nuclei are elongated, irregular in shape and are not arranged in a pattern within the glial lamina. Scale bar = 20 μm in panels C, F and I (applies to their respective rows); 20 μm in panel J.

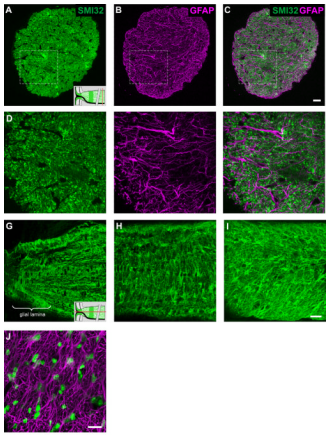

Fig. 3.

Transverse sections of the optic nerve within the myelinated region and labeled for SMI32 (A, D) and GFAP (B, E). Panels C and F show the colocalization pattern. The schematic of the optic nerve in the lower right-hand corner of panels A and G indicate where along the optic nerve the sections have been made (red bars). The honeycomb arrangement of the glial tubes is lost at the level of the myelinated nerve (A–C). Panels D–F depict an enlarged view of the area outlined by the dashed square in panels A–C, showing that there is less volume occupied by the astrocytes and their processes do not form distinct glial tubes (D–F). Panels G–I shows the progression in the disorganization of GFAP labeling in longitudinal section at various distances along the optic nerve (G, glial lamina; H, 300 μm; I, 3000 μm). (J) Single confocal transverse section of the myelinated region of the optic nerve labeled for GFAP and TOPRO. The cell nuclei within this region were small, round (compared to those in the glial lamina), and were not arranged in a pattern. Scale bar = 20 μm in panels C, F and I (applies to the respective rows); 20 μm in panel J.

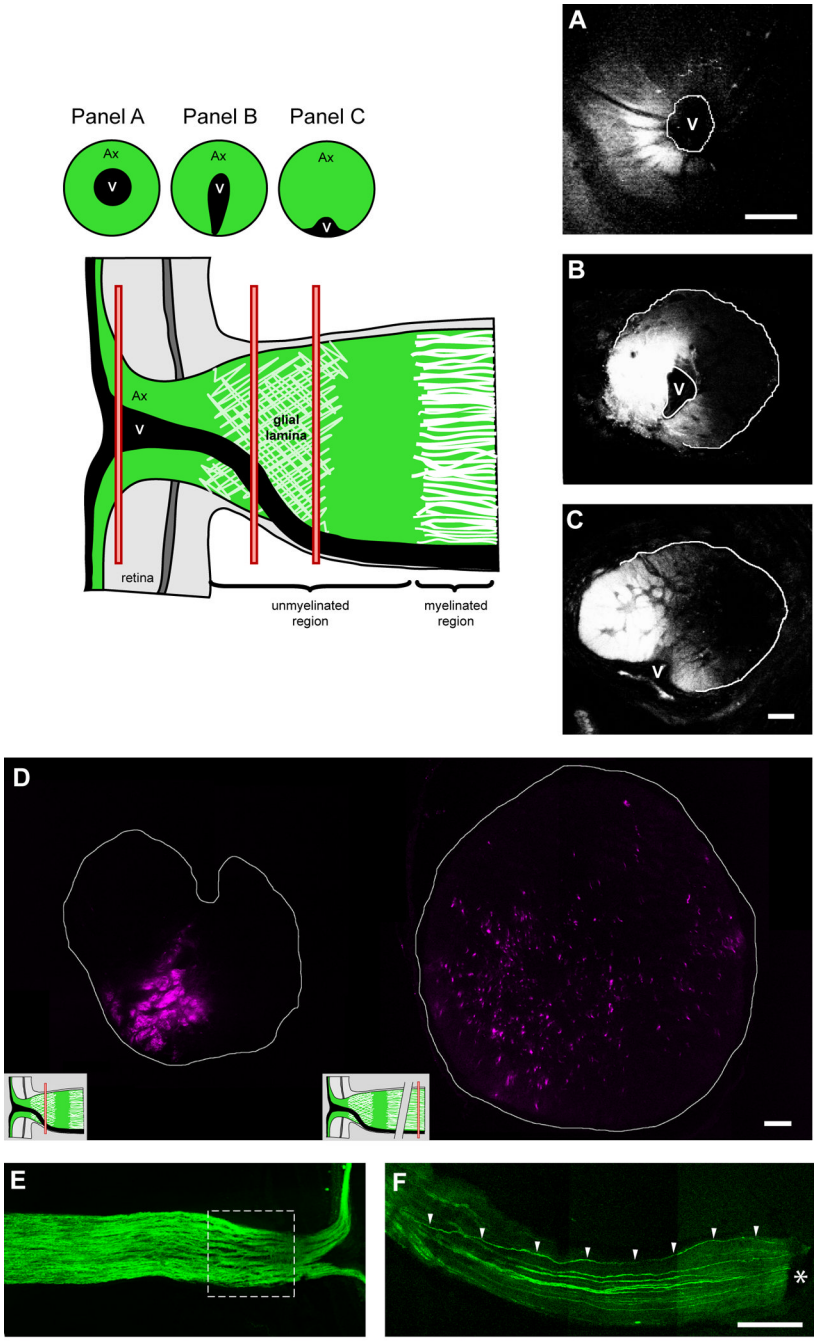

Fig. 4.

Transverse sections of the optic nerve showing ganglion cell axons that have been anterogradely labeled with DiI. Axon bundles within the optic nerve project topographically to specific regions of the retina (A–C; successive sections from the same optic nerve). The origin of the transverse sections in panels A–C is shown in the schematic (red bars). Panel D shows that at the level of the glial lamina (left image), axons are segregated into bundles, whilst further posteriorly along the optic nerve within the myelinated region (right image), the axons have dispersed and no longer maintain their spatial relationship. This is also discernible upon longitudinal section (E; dashed square represents the optic nerve head region). Further posteriorly, the bundles appear to coalesce. Using a transgenic mouse that

expresses GFP in sparse populations of ganglion cell axons (GFP-M), a traced axon is seen to deviate from it's original location at the periphery of the optic nerve (F; arrowheads). The asterisk depicts a remnant of the sclera/retinal pigment epithelium. Ax, axons; V, blood vessel. Scale bar = 100 μm in panel A; 20 μm in panel C (applies to panels B and C); 20 μm in panel D; 200 μm in panel F (applies to panels E and F).

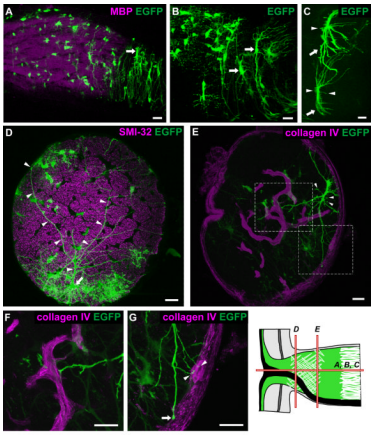

Fig. 5.

Longitudinal and transverse sections of hGFAPpr-EGFP optic nerve showing the morphology of astrocytes within the glial lamina. The schematic of the optic nerve head in the bottom right-hand corner of the figure depicts the origin of the sections shown in each panel. The glial lamina consisted predominantly of transversely oriented astrocytes with thick elongated cell bodies and primary processes extending long distances (A–C; arrows). The overall appearance of these astrocytes was that of a baseball catcher's mitt. Many small branches emanated from the cell body (C; arrows). Panel D shows an astrocyte (arrow) with processes (arrowheads) that extend the full width of the optic nerve, crossing numerous axon bundles to contact the pial wall via bulbous endfeet. In transverse section, the primary processes extend to contact the pial wall (E, G; arrows) or blood vessels (E, F, G; arrowheads), which have been labeled with collagen IV. Panels F and G represent an enlargement of the area in the dashed square in panel E. Scale bar in each panel = 20 μm.

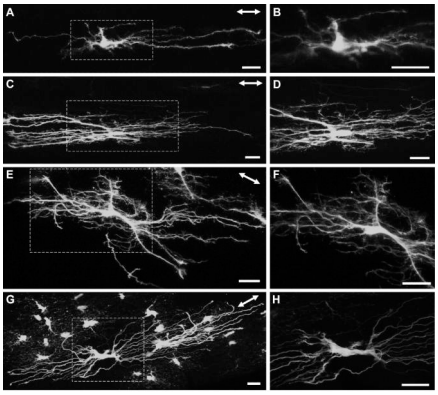

Fig. 6.

Longitudinally oriented astrocytes from the myelinated region of the hGFAPpr-EGFP optic nerve. The astrocytes depicted in this figure were located between the junction of the unmyelinated/myelinated region and approximately three to four millimeters posteriorly. The area represented by the dashed square in panels A, C, E and G are enlarged in panels B, D, F and H. There were numerous morphological varieties of longitudinally oriented astrocytes. Some exhibited very few primary processes that were straight and have few higher order branches (A, B), others possessed undulating processes with many collaterals and small offshoots, giving the astrocyte a ‘hairy’ appearance (C–F). One astrocyte possessed many primary processes, but showed very few higher order branching (G, H). The double-headed arrow in the top right corner of each panel indicates the direction of the long axis of the optic nerve. Scale bar in each panel = 20 μm.

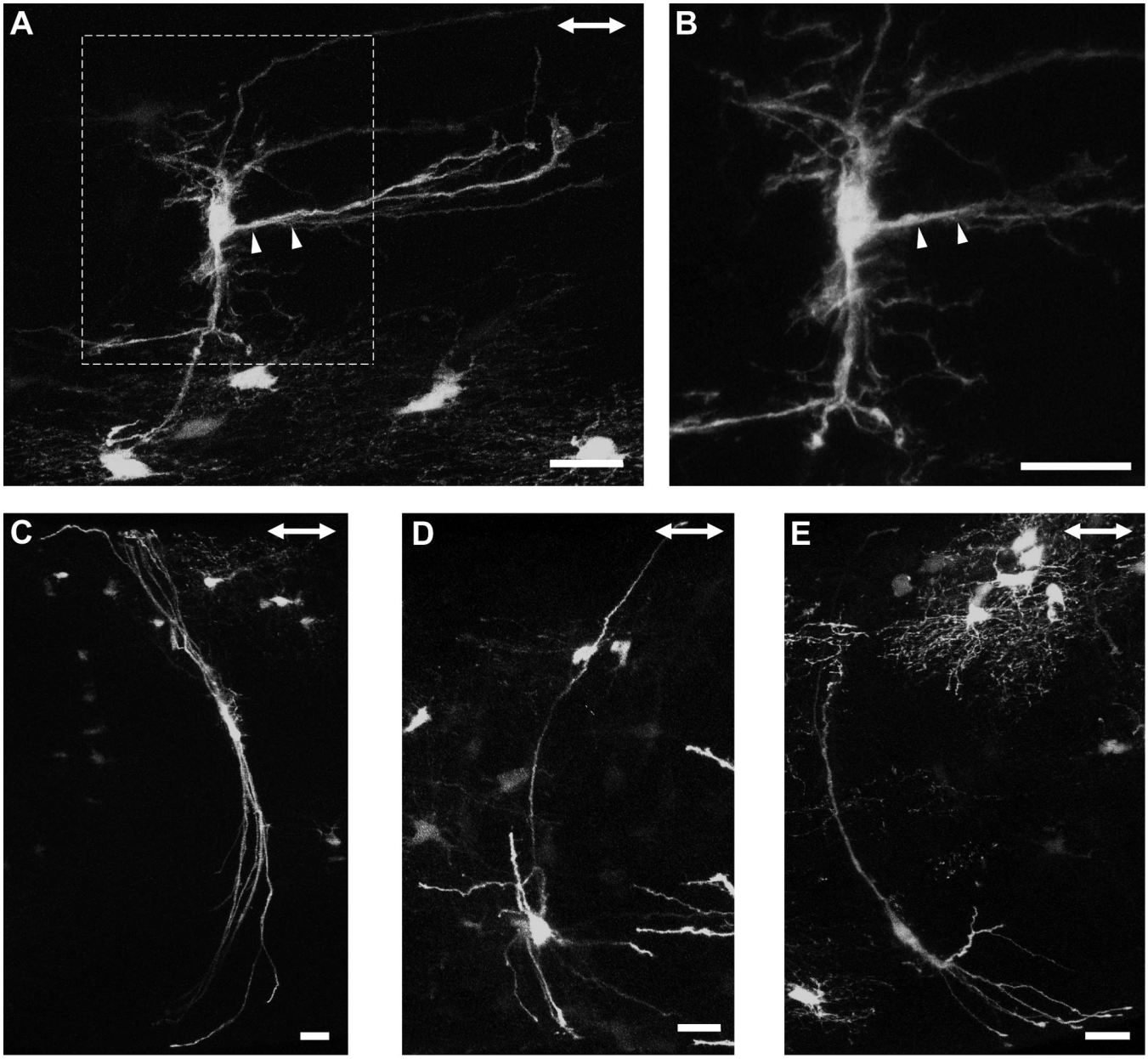

Fig. 7.

Transversely oriented astrocytes from the myelinated region of the hGFAPpr-EGFP optic nerve. The astrocytes depicted in this figure were located between the junction of the unmyelinated/myelinated region and approximately three to four millimeters posteriorly. One example of this astrocyte also projected a thick extensive longitudinal process (A, B). Others exhibited a thin elongated cell body with primary processes projecting straight to the pial wall. These astrocytes have very few higher order branches emanating from their cell bodies or primary processes (C–E). The double-headed arrow in the top right corner of each panel shows the direction of the long axis of the optic nerve. Scale bar in each panel = 20 μm.

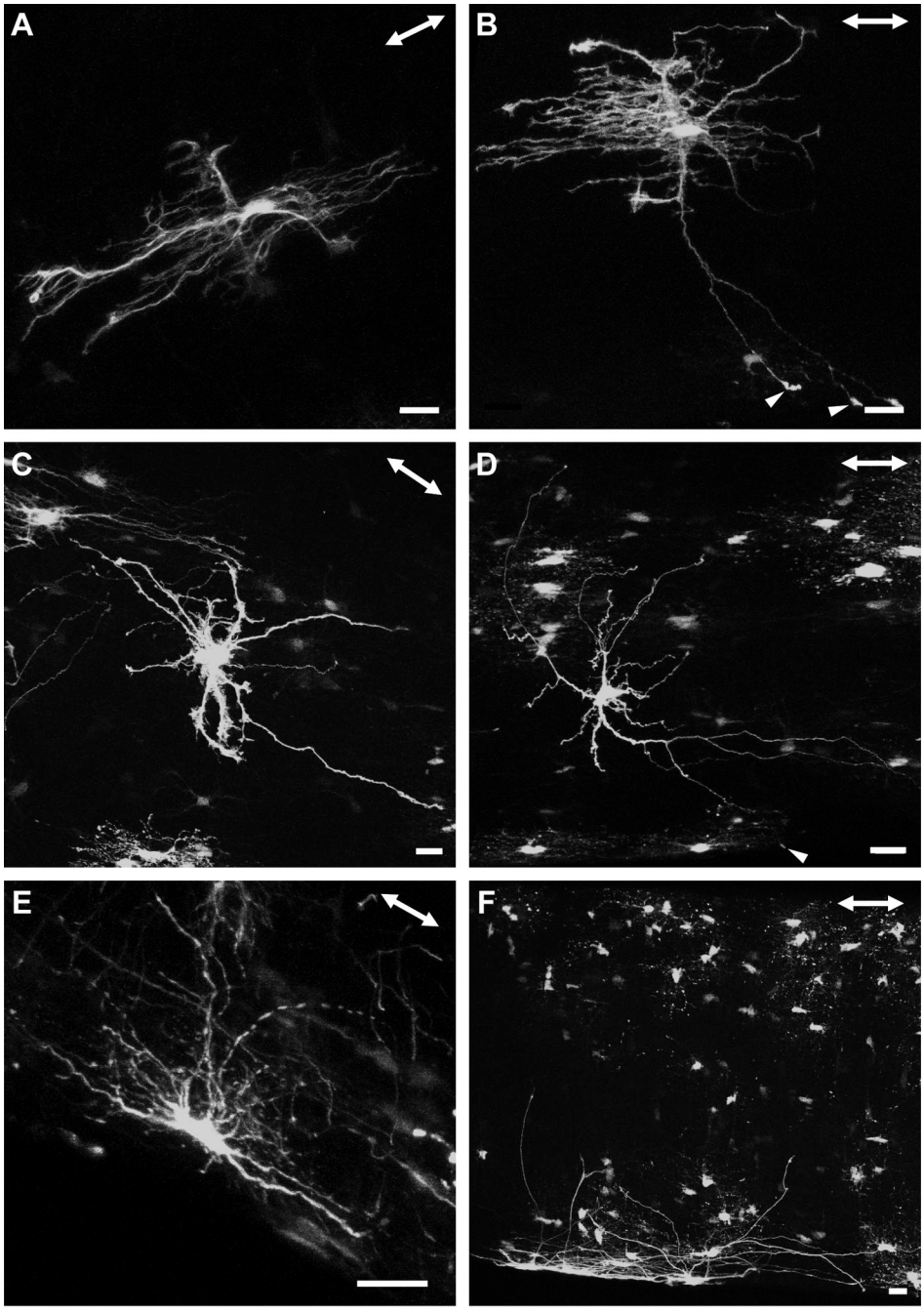

Fig. 8.

There were many morphological varieties of astrocytes, with some projecting primary processes in both the longitudinal and transverse direction (A, B), as well as in random directions (C, D). The primary processes of some of these astrocytes contacted the pial wall with bulbous endfeets (B, D, arrowheads). A gallery of additional examples is shown in the supplementary material (Fig. S2). There were some astrocytes with elongated cell bodies that lay in parallel with the long axis of the optic nerve, adjacent to the pial wall. The astrocytes depicted in this figure were located between the junction of the unmyelinated/myelinated region and approximately three to four millimeters posteriorly. The double-

headed arrow in the top right corner of each panel indicates the direction of the long axis of the optic nerve. Scale bar in each panel = 20 μm.

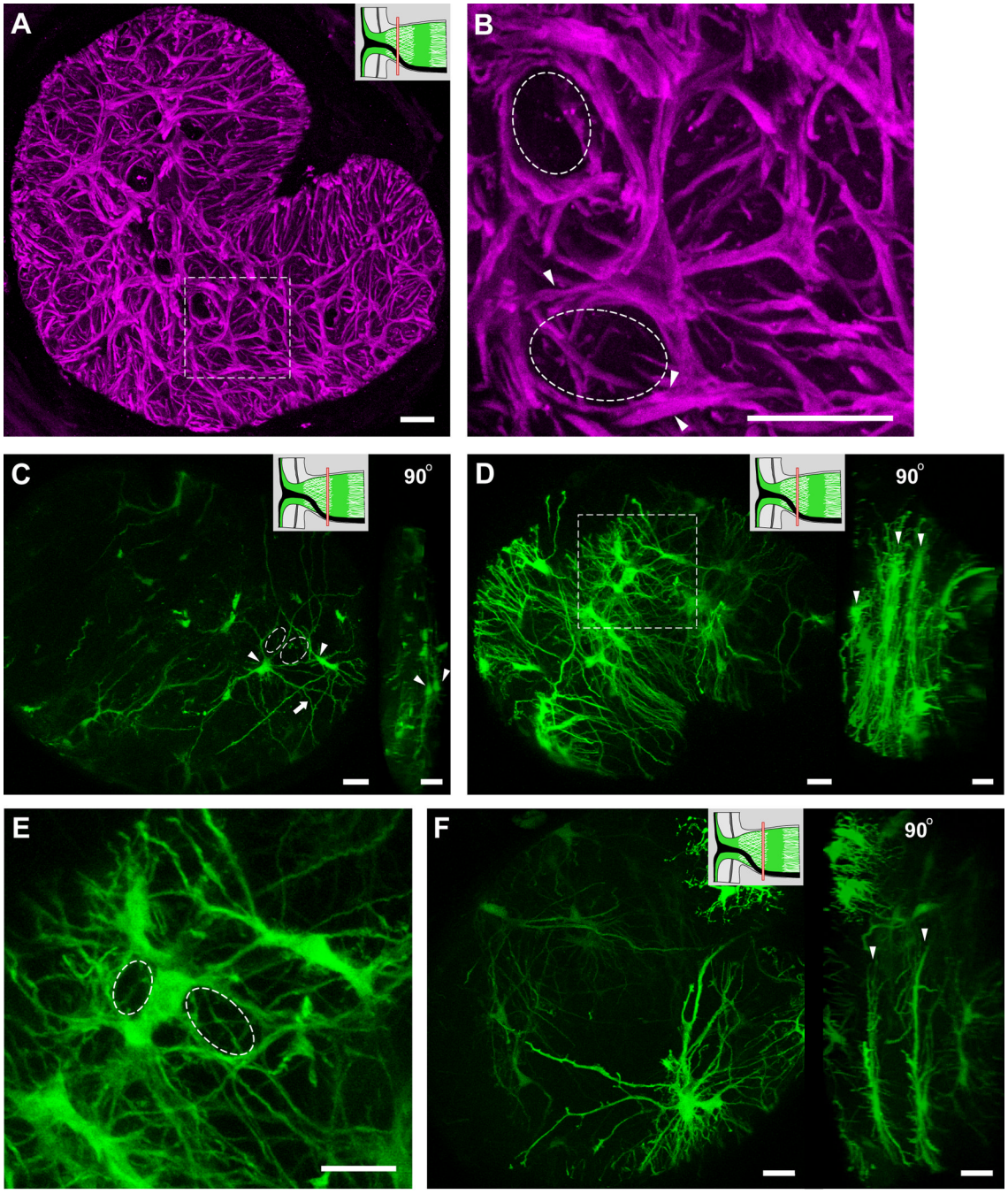

Fig. 9.

Transverse sections of GFAP labeled optic nerve showing that each of the glial tubes within the honeycomb structure are ensheathed by many astrocytic processes (A, B, dashed circles and arrowheads). Panel B shows an enlargement of the dashed square in panel A. (C) A section of hGFAPpr-EGFP optic nerve demonstrating the spatial organization of astrocytes within the glial lamina. The processes of two neighbouring astrocytes (arrowheads) can be seen to pass each other, forming holes through which ganglion cell axons pass through (dashed circles). A 90° rotation of the left image in panel C shows that the two astrocytes (arrowheads) lie close to each other in the same transverse plane. Because of the density of astrocytes and their far-reaching processes, astrocytes within the glial lamina do not tile and

each one may participate in forming the sheaths of many glial tubes, both near and distant. Panels D, E and F show examples of how many astrocyte cell bodies and processes overlap to form glial tubes (the dashed square in panel D is enlarged in panel E). Transversely oriented astrocytes within the glial lamina do not project extensive longitudinal processes and arrange themselves to form sheets of astrocytes (D and F, right image arrowheads). The schematic of the optic nerve head in the upper right-hand corner of panels A, C, D and F indicate where along the optic nerve the transverse sections have been made (red bars). Scale bar in each panel = 20 μm.

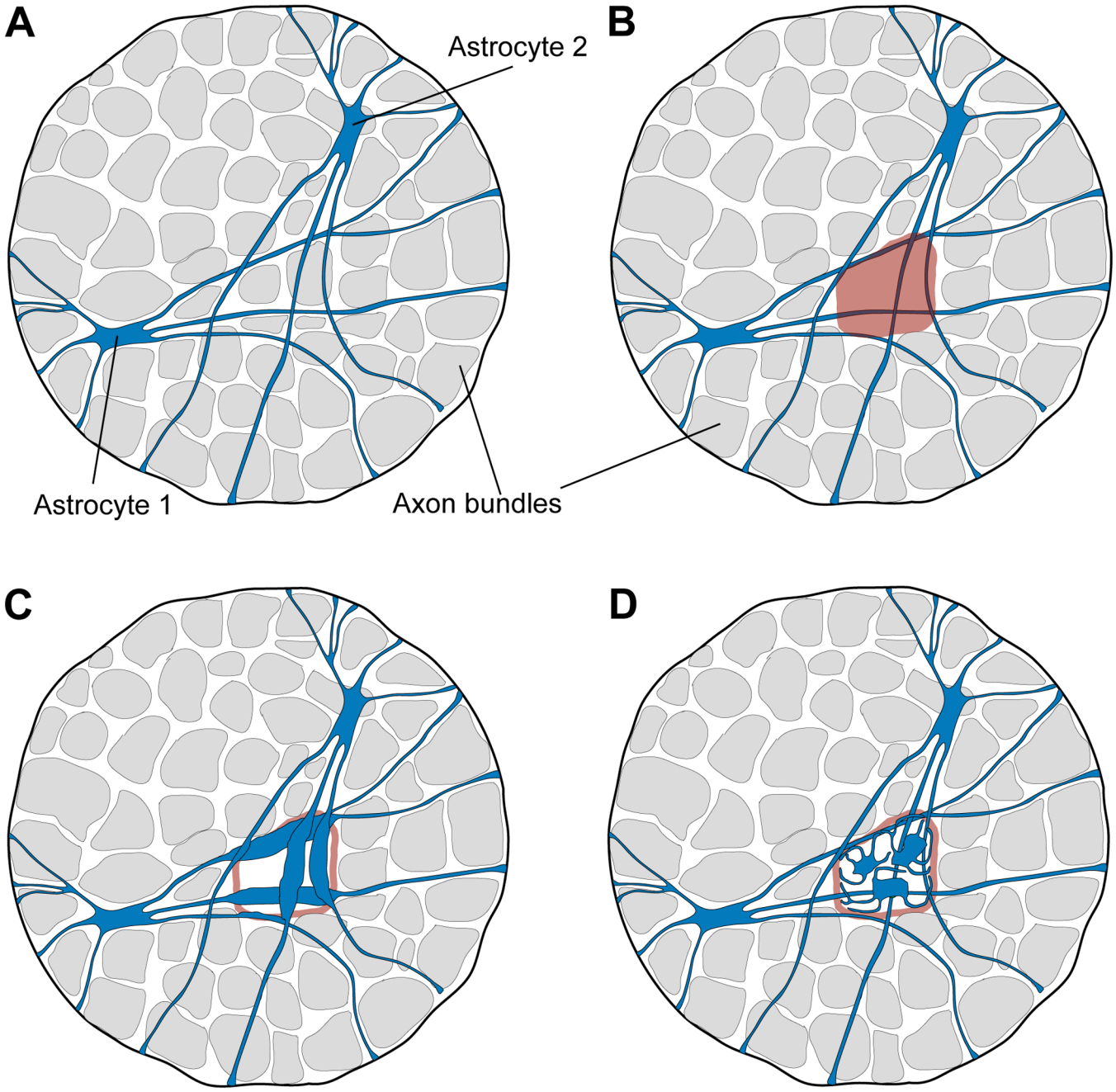

Fig. 10.

How do astrocytes come to fill the space vacated by axons that have degenerated? (A) Two astrocytes are illustrated. They spread widely across the glial lamina. (B) The degeneration of axons affects restricted, fan-shaped sectors of the retina, which represent focal bundles of damaged axons in the optic nerve. Such a focal region of nerve degeneration impinges on the processes of many astrocytes. And yet, the region of "gliosis" remains local – it appears to be confined to the region from which axons are lost (Fig 6 of Howell et al., 2007). (C) One way for glial reactivity to be restricted to the local region of axonal damage would be for upregulation of GFAP (the usual marker) to be confined to only a sector of each individual astrocyte. However, this would require a remarkable specificity of protein

targeting on the part of the astrocyte. (D) An alternative is that astrocytes divide and perhaps migrate to fill the vacated space. The molecular cues that would guide this process appear to be unknown.

Table 1

Primary antibodies used in this study.

Primary Antibody	Antigen	Immunogen	Source	Dilution
SMI32	Neurofilament heavy non-phosphorylated	hippocampal protein extract	Covance (Emeryville, CA), mouse monoclonal, #SMI-32R, lot #9	1:400
GFAP	Glial fibrillary acidic protein	GFAP purified from normal human brain	Sigma (St Louis, MO), rabbit polyclonal, #G9269	1:400
MBP	Myelin basic Protein	Human MBP isolated from normal human brain. Rat monoclonal raised against full length bovine MBP.	Abcam (Cambridge, MA), rabbit polyclonal (#ab12355-50, lot #212221) or rat monoclonal (#ab7349-2, lot #226183)	1:400
NG2	NG2 chondroitin sulfate proteoglycan	Immunoaffinity purified NG2 chondroitin sulfate proteoglycans from rat	Chemicon (Billerica, MA), rabbit polyclonal, #ab5320, lot #LV1361596	1:400
APC	Adenomatus polyposis coli	Recombinant protein consisting of amino acids 1–226 of APC	Calbiochem (San Diego, CA), mouse monoclonal, #OP80, lot #D35078	1:200
Collagen IV	Collagen Type IV	Human and bovine placental collagen IV	Chemicon (Billerica, MA),goat polyclonal,#ab769, lot#24020212	1:400

Table 2

The total number of axon bundles traversed by the processes of an individual astrocyte from the glial lamina.

Astrocyte	Total number of axon bundles passed by the processes	Total number of axon bundles*
1	21	85
2	19	80
3	23	87
4	28	92
5	18	83
6	17	95
Average	21	87

*This number represents the total number of axon bundles counted for a given transverse section of the glial lamina. We have taken the transverse section from the same region of the glial lamina in all samples. Each astrocyte was derived from independent samples.